Journal Name

ARTICLE

A DFT and Multi-configurational Perturbation Theory Study on O_2 Binding to a Model Heme Compound via the Spin-change Barrier

Received 00th January 20xx,
Accepted 00th January 20xx

DOI: 10.1039/x0xx00000x

www.rsc.org/

Y. Kitagawa,[a] Y. Chen,[a] N. Nakatani,[a] A. Nakayama[a] and J. Hasegawa[a,b,*]

Dioxygen binding to a model heme compound via intersystem crossing (ISC) was investigated with multi-state multi-configurational self-consistent field with second-order perturbation theory (MS-CASPT2) and density functional theory (DFT) calculations. In elongated Fe-O distances, the energy levels of the S_0 and T_1 states are separated, which decreases the probability of intersystem crossing in these structures. At the DFT(B97D) level of calculation, the Fe-O distances of the S_0 and T_1 states were 1.91 and 2.92 Å , respectively. Minimum energy intersystem crossing point (MEISCP) was located as a transition state at Fe-O distance of 2.17 Å with the energy barrier of 1.0 kcal/mol from T_1 minimum. The result was verified with MS-CASPT2 calculations including spin-orbit interaction which also showed the intersystem crossing point at Fe-O distance of 2.05 Å. An energy decomposition analysis on the reaction coordinate showed the important contribution of the ring-shrinking mode of the porphyrin ring, indicating that the reaction coordinates which control the relative energy level of the spin-states play a key role in the intersystem crossing.

1. Introduction

Dioxygen (O_2) binding to hemoglobin and myoglobin is one of the most important molecular processes of the living animals. The electronic structure of the Fe-O_2 bonding has been studied for many decades (see review articles, for example references [1] and [2]). As pointed out in 1936 by Pauling,[3] the electronic ground-state of heme in the O_2-free form (deoxyheme) is quintet spin state, while that of the O_2-attached form (oxyheme) is singlet state. The O_2 binding process, therefore, involves intersystem crossing (ISC). Among several phases in the O_2 binding observed by the experiments,[4-6] we focus on the fast O_2 binding process.

$$\text{Deoxyheme (S=2)} + O_2\ (S=1) \longrightarrow \text{Oxyheme (S=0)} \qquad (1)$$

Even though there are a number of studies on the nature of the Fe-O_2 bonding[2, 3, 7-16], less number of papers reported potential energy surface of the O_2 binding.[14, 17-21] In these reports, two kinds of ISC mechanisms were discussed. The first one is so-called broad-crossing mechanism.[17-19] According to the Density Functional Theory (DFT) calculations, potential energies of oxyheme in singlet, triplet, and quintet states are nearly degenerate, and their slopes are similar at large Fe-O_2 distances (more than 3 Å). On the basis of Landau-Zener equation, these features of the potential energy surfaces enhance ISC.[18] However, this mechanism, which is based on the near degeneracy in the long Fe-O distances, is inconsistent with the stability of the quintet state in deoxyheme. As reported elsewhere, the relative energy between spin states depends on the exchange-correlation functional adopted in the DFT calculation.[22, 23]

The second mechanism states that the singlet-triplet crossing point becomes a transition state (TS) in the O_2 binding process. The energy barrier to cross a TS of this type was termed as "spin-change barrier"[24] and "two-state-reactivity".[25, 26] Novoa et al. reported CASPT2 calculations for the Fe(O_2)-Porphyrin-Imidazole system. The singlet-state structures, which were optimized with DFT(BP86), were used for the single-point CASPT2 calculations for both singlet and triplet states.[14] Calculated O_2 binding energy was 14.9 kcal/mol, which reasonably agrees with the experimental observation.[27] They found a van der Waals (vdW) minimum at Fe-O distance of 2.6 Å in the triplet-state surface. To reach S_0 minimum, the triplet potential curve has to go through an ISC point between the triplet and singlet states, $(T_1/S_0)^{ISC}$, at the Fe-O distance of 1.9 Å. In our previous study, we performed B3LYP calculations to draw two-dimensional potential surface, and showed that the spin-change barrier creates a transition state.[20]

Another point of interest is the reaction coordinate of the spin-crossing reactions, particularly for the spin-barrier case. In a single adiabatic potential surface, a transition state arises from the intersection of two diabatic states. Many of the elementary processes are described with a single reaction coordinate such as a bond length. On the other hand, a

[a] Institute for Catalysis, Hokkaido University, Kita 21, Nishi 10, Kita-ku, Sapporo, Hokkaido 001-0021, Japan.
[b] JST-CREST.

† Footnotes relating to the title and/or authors should appear here.
Electronic Supplementary Information (ESI) available: Result of the xc-functional investigation, 2D potential curve by B3LYP. Atomic coordinates for the energy minimum structures for S_0 and T_1 states and (S_0/T_1) MEISCP. Some important natural orbitals and their occupation number calculated with DFT(B97D) at the S_0 and T_1 structures. See DOI: 10.1039/x0xx00000x

transition state of the ISC is defined by the relative energy of two different spin states. Therefore, an elementary reaction step could involve two reaction coordinates; one for the bond formation and the other for the relative energy between the two spin states. This fact enhances the importance to locate the transition state of the intersystem crossing to understand the detail of the reaction mechanism as recognized in pioneering studies.[28, 29]

In the present study, we revisited potential energy surface of the O_2 binding at a model Heme compound, Fe^{II}-porphyrin-imidazole, using the density-functional theory (DFT) and restricted active space second-order perturbation theoretical (RASPT2) method. After computational details are described in the next section, RASPT2 potential energy curves for the singlet and triplet states are explained in the third section. With the B97D[30, 31] functional that includes vdW interactions, we optimized the structure of the lowest energy spin state at a given structure. The RASPT2 calculations followed, and the result showed that the intersection of the singlet and triplet surfaces produces an energy barrier, so-called spin-change barrier, at the structure closer to the O_2 binding equilibrium than those indicated by the broad-crossing mechanism. In the fifth section, potential energy surfaces in one- and two-dimensional surfaces were investigated. A minimum energy intersystem crossing point (MEISCP) was located and confirmed to be a transition state in this spin-changing reaction. Before the conclusion is given, we show the result of an energy-decomposition analysis for investigating the reaction coordinate that effectively connects the T_1 minimum to the MEISCP.

2. Computational details

A computational model of oxyheme ($FeC_{23}N_4O_2H_{16}$) is composed of iron(II) porphyrin ($FeC_{20}N_4H_{12}$) with imidazole ($C_3N_2H_4$) ligand as shown in Figure 1. Hereafter, the structures of oxyheme and deoxyheme are also denoted as $Fe(O_2)$PorIm and FePorIm, respectively.

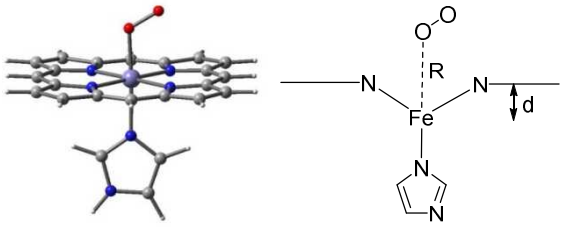

Figure 1 Computational model of oxyheme, the $Fe(O_2)$PorIm complex. "R" and "d" denote the Fe-O distance and out-of-displacement of Fe atom. The latter was defined as distance between Fe and the mass-centre of four N atoms.

Applicability of the exchange-correlation functionals in the DFT calculations was examined before the structural optimization. Because the Fe-O distance in the singlet and triplet states is similar to that reported in the previous CASPT2 result,[14] B97D functional was adopted. For the results, see Figure S1 in Electronic Supplementary Information (ESI). Our result is corroborated by a previous report in which the B97D showed a fine performance in calculating 3d transition metal complexes.[31] The basis sets used for the optimization was Stuttgart/Dresden (SDD) sets of the effective-core potential and valence basis sets for Fe,[32] the 6-311+G* sets for the O and N atoms,[33] 6-311G* for the C atoms,[33] 6-31G** for the H atoms.[34] The basis sets used for the RASPT2 calculation were ANORCC[35, 36] sets, 6s5p4d3f2g for Fe, 4s3p2d for O and N, 3s2p1d for C, and 2s for H atoms. In the RASPT2 calculations, we first obtained state-averaged(SA)-(10e,13o)-CASSCF in which three singlet states and three triplet states were equally weighted. The CASSCF active orbitals were composed of five 3d orbitals of Fe and their double-shell counterpart, a set of oxygen anti-bonding π orbitals, $\pi^*_\perp$ and $\pi^*_\parallel$ and one 2pσ type orbitals of the N atoms in porphyrin. These CASSCF orbitals were used for the (26e, 22o)-RASPT2 calculations. In the RASPT2 calculations, the active space was as follows. For the RAS1 space, where two electrons were taken out, we adopted 3s, 3p orbitals of Fe, 2pσ and 2pπ bonding orbitals of oxygen, one 2pσ type orbitals of the N atoms in porphyrin, one 2pσ type orbitals of the N atoms in imidazole. For the RAS2 space, five 3d orbitals of Fe and a set of oxygen anti-bonding π orbitals were adopted. For the RAS3 space, to which two electrons were promoted, we adopted five double-shell counterpart of Fe 3d orbitals, and anti-bonding 2pσ* orbitals of oxygen. In this RAS step, RAS Self-Consistent Field calculation was approximated by RAS Configuration Interaction calculation because the orbitals were optimized once in the SA-(10e,13o)-CASSCF step. For the PT2 calculations, imaginary shift[37] of 0.1 au was applied.

We also performed MS-(14e, 10o)-CASPT2 calculations to confirm the steepest-descent-type IRC calculation with the B97D functional. ANO-RCC basis sets were used: 6s5p3d1f for Fe, 3s2p1d for O, 3s2p1d for N, 2s for H, 3s2p for other C and N. The active space was composed of $3d_{x^2-y^2}$ and its double-shell counterpart, $3d_{xz}$, $3d_{yz}$, $3d_{xy}$, $3d_{z^2}$, bonding and anti-bonding π orbitals of O_2.

MEISCP between the spin states was determined by using an in-house program package developed by Nakayama et al.[38] A constraint optimization method developed by Martinez and co-workers[39] was used.

The DFT calculations were performed with Gaussian09 package,[40] and the CASSCF and RASPT2 calculations were with MOLPRO[41, 42] and MOLCAS[43] programs.

3. RASPT2 potential curve for the O_2 binding

For each ground state in the singlet and triple spin multiplicity, relaxed potential energy scan calculations were performed with fixed Fe-O distances at the B97D levels. Single-point RASPT2 calculations were performed at the B97D optimized structures. The result is qualitatively the same as the previous CASPT2 calculation[14] as shown in Figure 2. At the long Fe-O distances, the ground-state spin-multiplicity is triplet, and the single-triplet energy gap was about 16 kcal/mol at 2.9 Å. The triplet-state curve has the lowest energy point at 2.4 Å.

At shorter Fe-O distances, the singlet-triplet gap shrinks rapidly and becomes about 8 kcal/mol at 2.1 Å. The T_1@T_1 and S_0@T_1 lines finally cross each other at 1.9-2.0 Å. For Fe-O distances shorter than 2.0 Å, the structures were switched to the singlet-optimized one. The singlet-state potential curve has an energy minimum at 1.9 Å, while the triple-state one monotonically increases in this region. In these potential curves, activation energy for the Fe-O bond formation is estimated about 7 kcal/mol. Even though the structure is based on DFT calculations, it is reasonable to consider that ISC occurs in this region with a certain amount of activation energy. This means that our present calculations support the spin-change barrier mechanism rather than the broad crossing mechanism. Therefore, we extend our discussion on the potential energy surface on the basis of the spin-change barrier mechanism in the following sections.

In the previous CASPT2 calculation, the energy minimum of the triplet state is by 2 kcal/mol lower than that of the singlet one.[14] In our present CASPT2 calculation, the energies of the singlet and triplet states are almost degenerate. The protein environment effect could stabilize the singlet state more than triplet state as stated previously.[2]

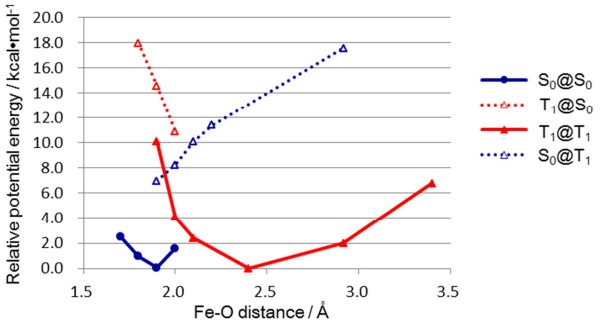

Figure 2. RASPT2 potential energy curves for the O_2 binding to the FePorIm complex. The "S_0@S_0" and "T_1@S_0" lines respectively denote the single-point calculation for singlet and triplet states at the singlet optimized structure. The "S_0@T_1" and "T_1@T_1" respectively denote the single-point calculations for singlet and triplet states at the triplet optimized structure.

4. Electronic structures of the singlet and triplet states

Electronic structure of the present CASSCF wave functions is explained very briefly. For a comprehensive explanation, please see previous studies.[2, 13, 15, 17, 44, 45] As in the previous studies, the ground state of Fe(O_2)PorIm obtained in the present study is a mixed Pauling and Weiss model. The most important component that has the largest weight is

$$\left(\pi_{\parallel}^{*}+d_{z^2}\right)^2(\pi_{\perp}^{*})^1\left(d_{xy}\right)^2\left(d_{yz}\right)^1(d_{xz})^2\left(d_{x^2-y^2}\right)^0\left(\pi_{\parallel}^{*}-d_{z^2}\right)^0.$$

Numbers in superscript are the occupation number In Figure 3a, some important MOs from SA-CASSCF calculation were given. The doubly occupied MO with the $\left(\pi_{\parallel}^{*}+d_{z^2}\right)$ character indicates the Pauling's component in the bonding. The $\pi_{\perp}^{*}$ and d_{yz} orbitals are singly occupied, and the d_{yz} orbital has some $\pi_{\perp}^{*}$ component. This indicate singlet coupling between these MOs, are the Weiss's component.[2, 15, 44] The later component, if the $\pi_{\perp}^{*}$ and d_{yz} MOs are represented by delocalized $\left(\pi_{\perp}^{*}+d_{yz}\right)$ and $\left(\pi_{\perp}^{*}-d_{yz}\right)$ MOs, the electronic structure is described with the linear combination of the $\left(\pi_{\perp}^{*}+d_{yz}\right)^2\left(\pi_{\perp}^{*}-d_{yz}\right)^0$ and $\left(\pi_{\perp}^{*}+d_{yz}\right)^0\left(\pi_{\perp}^{*}-d_{yz}\right)^2$.[2, 15, 44]

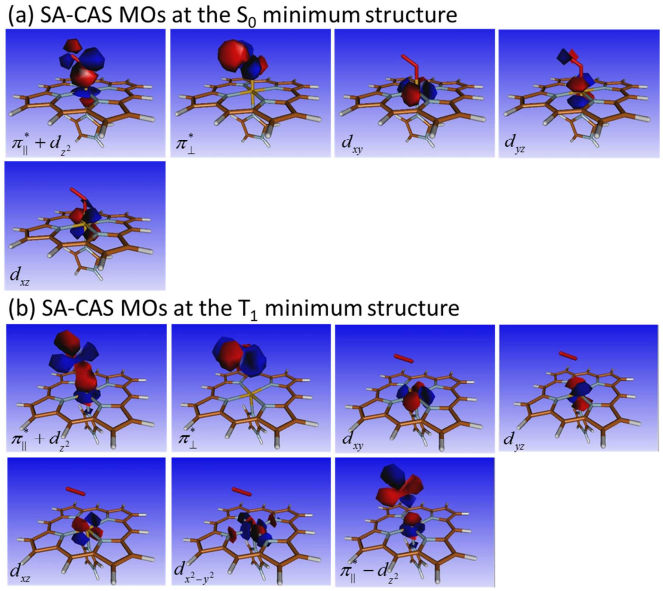

Figure 3 SA-CASSCF MOs at (a)S_0 and (b) T_1 energy minimum structures.

For the electronic structure of the T_1 state at the T_1-energy minimum, one of the most important components is as follows.

$$\left(\pi_{\parallel}^{*}+d_{z^2}\right)^2(\pi_{\perp}^{*})^1\left(d_{xy}\right)^1\left(d_{yz}\right)^1(d_{xz})^2\left(d_{x^2-y^2}\right)^1\left(\pi_{\parallel}^{*}-d_{z^2}\right)^0.$$

Compared with the determinant in the S_0 one, one-electron at the d_{xy} MO is promoted to $d_{x^2-y^2}$ with spin flip. The second important determinant includes 2 electron promotion from $\left(\pi_{\parallel}^{*}+d_{z^2}\right)$ MO to $\left(\pi_{\parallel}^{*}-d_{z^2}\right)$ MO. The σ bonding by the Pauling configurations were, therefore, weakened because of the elongated Fe-O distance at the T_1 minimum.

5. Potential energy surface and minimum energy intersystem crossing point by DFT calculations

Here, we discuss potential energy surface calculated by DFT with the B97D functional. We also explain the molecular structure at the MEISC point that corresponds transition state in adiabatic reactions. The B97D calculated potential curves are shown in Figure 4. For each Fe-O distance, other structural parameters were optimized.

In the dissociation limit, the triplet state (T_1@T_1) is lower than the singlet state at the triplet-optimized geometry (S_0@T_1) by 9 kcal/mol and at the singlet-optimized geometry (S_0@S_0) by 5 kcal/mol. These data correspond to the relative energy of spin states in deoxyheme, and the result agrees reasonably well with the previous CASPT2 level calculation.[45, 46] As seen in Figure 4, the triplet ground state has an energy

minimum at Fe-O of 2.917 Å. At the T_1 minimum geometry, the lowest singlet state (S_0@T_1) is still higher than the T_1 state by 8 kcal/mol. As seen in Figure 2, the present RASPT2 calculations at the T_1 minimum gave the energy difference of about 13 kcal/mol which is by about 5 kcal/mol larger than the B97D one. At shorter Fe-O distances, the gap between the singlet and triplet states decreases rapidly and becomes zero at the Fe-O distance of 2.0 Å. This ISC point is by 2 kcal/mol higher than the T_1 minimum structure.

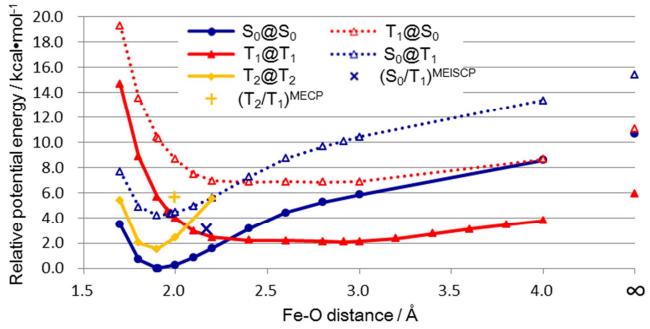

Figure 4 Result of the B97D scan calculations for O_2 binding to FePorIm complex. "X@S_0", "X@T_1", and "X@T_2" (X=S_0, T_1, and T_2) denote that the structure is optimized for the S_0, T_1, and T_2 states, respectively. "$(S_0/T_1)^{MEISCP}$" and "$(T_2/T_1)^{MECP}$" denote the MEISC point and the minimum energy crossing point (MECP), respectively.

On the other hand, the singlet ground state has an energy minimum at the Fe-O distance of 1.907 Å, which is by 2 kcal/mol lower than the T_1 minimum. The calculated O_2 binding energy is about 6 kcal/mol which is in qualitative agreement with the experimental data of 10.1 kcal/mol (corrected value[45]). We also note that there is another low lying triplet state (T_2 in Figure 4). The electronic structure is unpaired electrons at the $(\pi_{\perp}^{*} + d_{yz})$ and $(\pi_{\perp}^{*} - d_{yz})$ MOs.

As it is well known, the two hypersurfaces intersect as a seam of crossing. There is a minimum energy point along the seam. Even though the singlet and triplet states crosses at Fe-O of 2.0 Å in Figure 4, this is not necessarily the MEISCP. Optimizing the structure on the crossing seam, we found the MEISCP at the longer Fe-O distance (2.17 Å). This structure is a transition state of O_2 bonding via the spin barrier. The activation energy was calculated to be just 1.0 kcal/mol. As shown later, energy surface of the singlet state rapidly decreases towards the singlet energy minimum structure in this structures.

We also located a T_1/T_2 minimum energy crossing point (MECP) at Fe-O distance at 2.0 Å. This MECP is by 3.5 kcal/mol higher than the T_1 minimum. Concerning the O_2 binding reaction pathway, the (S_0/T_1) MEISCP, which is lower than the (T_2/T_1) MECP, is expected to be a preferable pathway.

Figure 5 (a, b) shows two-dimensional potential curves for the O_2 binding via ISC at the B97D level. In Figure 5(a), the reaction pathway from dissociation limit to the ISC was calculated with the Fe-O distance as reaction coordinate. T_1 state has the energy minimum at 2.92 Å. The O_2 binding energy is 3.87 kcal/mol. At the shorter Fe-O distances less than 2.0 Å, the energy of the T_1 state raises rapidly and reaches the ISC point at the Fe-O distance of 1.975 Å. The activation energy to reach the ISC is 2.28 kcal/mol from the T_1 minimum. After the ISC, the energy of oxyheme in the S_0 state monotonically decreases along the steepest decent pathway. The energy minimum was located at the Fe-O distance of 1.907 Å. Therefore, along the pathway, the ISC point does not appear until the Fe-O distance becomes close to that of the S_0 minimum.

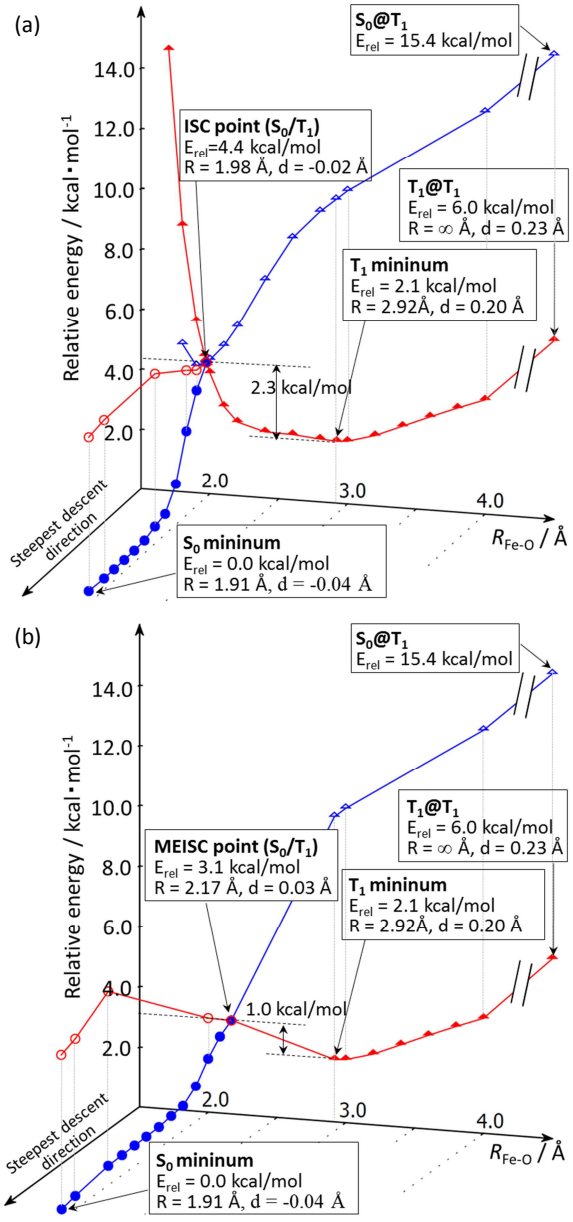

Figure 5. Two dimensional potential energy curves for O_2 binding calculated at the B97D level. (a) Intersystem crossing pathway along the Fe-O fixed coordinate and (b) that via the MEISCP. Triangle denotes that the calculations were performed with fixed Fe-O distances. Filled triangles denote that the structure was optimized with this triplet state, while open triangles denote single-point energy. Filled circles denote that the steepest decent reaction pathway on the S_0 surface starting with the ISC point, while open circles denote single-point calculations.

Figure 5(b) shows a reaction pathway through the MEISCP that was located just above 1.02 kcal/mol from the T_1 energy minimum. The MEISCP is a transition state of the spin crossing

reaction pathway. This activation energy is by 1.26 kcal/mol smaller than that of the ISC pathway. The Fe-O distance is 2.167 Å, which is about 0.2 Å longer than that of the ISC point as seen in Figure 5(a). From the MEISCP, so-called meta-Intrinsic Reaction Coordinate (mIRC) calculations were performed toward the S_0 minimum. Along the pathway after the MEISCP, the energy of the S_0 state monotonically decreases and reaches to the energy minimum along the steepest decent pathway. Structure changes after passing the MEISCP are mainly in the Fe-O_2 distance, and the Fe ion is already in the porphyrin plain at the MEISCP.

There are some comments that DFT calculations for the transition metal should use hybrid exchange-correlation functional.[23] We also performed the same calculations for the two dimensional surfaces with the B3LYP functional (see Figure S2 in SI). The result was similar to that obtained with the B97D functional. The T_1 minimum was located at the Fe-O_2 distance of 3.03 Å, which was about 0.1 Å longer than that obtained with B97D. The barrier height to the ISC point and MEISCP were 4.06 and 2.42 kcal/mol, respectively, which are again qualitatively similar to the B97D result. The MEISCP was located at Fe-O_2 distance of 2.78 Å, which is by 0.6 Å longer than that with the B97D result.

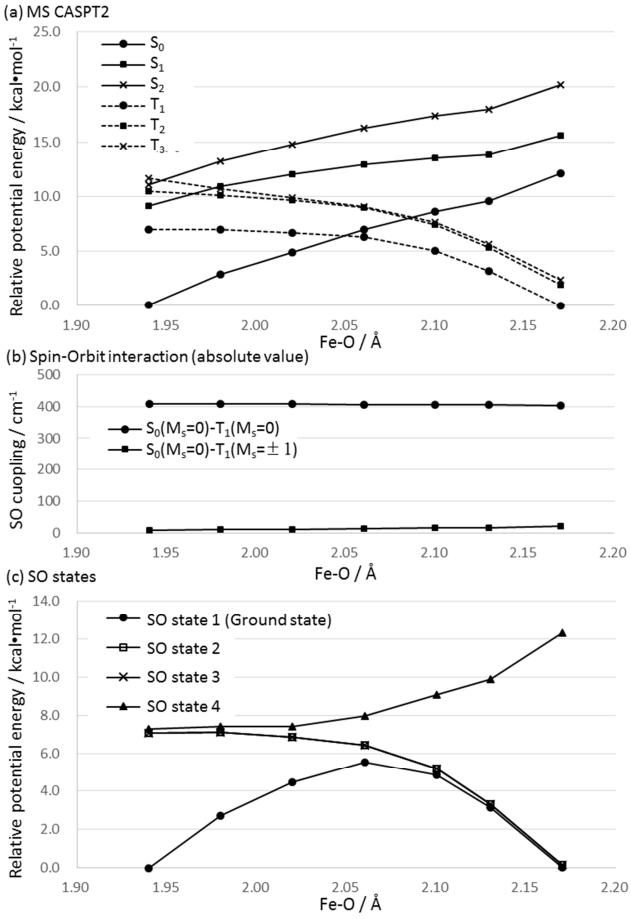

Figure 8 (a) MS-CASPT2 potential energy curves around the MEISCP between the lowest singlet and triplet states. (b) Magnitude of the spin-orbit interaction between the lowest singlet and triplet states around the MEISCP. (c) Eigenstates of the SO Hamiltonian described with the MS-CASPT2 states.

There are also discussion about the dispersion effect on the O_2 binding energy. In previous study,[23] the empirical dispersion effect[31] was examined for the B3LYP and B3LYP* functionals. In their result, the binding energy increased by 7.7 kcal/mol for both two functionals. In the present case, the B97D result was compared with the B971,[47] because the B97 was not available right now. The B971 case, the binding energy was 5.3 kcal/mol, which is 0.7 kcal/mol less than the B97D case. The experimental binding energy was reported to be 10.2 kcal/mol and 12.3 kcal/mol,[23] and the dispersion treatment modified the binding energy to the correct direction. For the T_1 minimum, the B971 binding energy was 3.6 kcal/mol, which is by 0.3 kcal/mol less than the B97D one. This also shows the same trend.

To verify the DFT description of the O_2 binding pathway, single-point calculations with the MS-CASPT2 method were performed at structures around the MEISCP. The procedure is as follows. We first performed mIRC calculation at the B97D level starting from the MEISCP. To the directions toward T_1 and S_0 minimum, triplet and singlet calculations were performed, respectively. Single-point calculations were performed at the MS-CASPT2 level. The results of 7 points are shown in Figure 8a. The potential curves of the lowest singlet and triplet states cross at around Fe-O distance of 2.05 Å, which is close to that of the MEISCP (2.17 Å) obtained with B97D. The result qualitatively supports the O_2 binding pathway obtained with B97D and B3LYP calculations. To understand the interactions between the lowest singlet and triplet states, we calculated the spin-orbit (SO) coupling. As shown in Figure 8b, calculated SO coupling was almost constant among the structures along the reaction pathway. Between the S_0 and T_1 states with M_s=0, the SO coupling was about 400 cm^{-1}, while that between singlet (M_s=0) and triplet (M_s=±1) states were negligibly small. We also diagonalized SO CAS State Interaction Hamiltonian.[48, 49] As shown in Figure 8c, the resultant potential curves show avoided crossing, and the ISC point becomes a transition state. From the right to the left of the transition state, the character of the lowest state changes from triplet-like to singlet-like state; see Figure 8c. The highest state behaves oppositely. Two states in the middle are degenerated and composed of triplet states with M_s = +1 and -1.

6. Reaction coordinate from T_1 minimum to MEISCP

In the previous section, we discussed mIRC pathway from the MEISCP. Here we introduce another view point. Because FePorIm initially binds O_2 at the T_1 minimum, we consider vibration at the T_1 minimum and investigated which normal mode effectively leads to the MEISCP. In the first step, normal mode analysis was performed at the T_1 minimum. In the second step, the structural changes that occur from the T_1 minimum to the MEISCP were expressed by the linear combination of the normal mode vectors. Finally, the energy change due to each normal mode was evaluated. For each scaled normal mode vector, the changes in the atomic

coordinates were applied to the T_1 minimum structure, and single-point calculation was performed to evaluate the energy contribution of each component. The analysis was performed for the B3LYP potential energy surface (Figure S2 in ESI).

The result is shown in Figure 9. The largest component was the 9-th vector whose coefficient was -0.41. As shown in Figure 10, the structural change induced by the 9-th mode is that the Fe atom moves closer to the porphyrin plane, and Fe-O_2 becomes shorter. As shown in Figure 9, Even though this is one of the most significant structure changes from deoxyheme to oxyheme, this change only stabilizes singlet state by 1 kcal and destabilizes triplet state by less than 0.5 kcal/mol. The 18-th component has an expansion coefficient of 0.17, and its energetic contribution was similar to that of the 9-th component. This component induces anti-symmetric shrinking of tetrapyrrole units accompanied by the Fe-O_2 stretching.

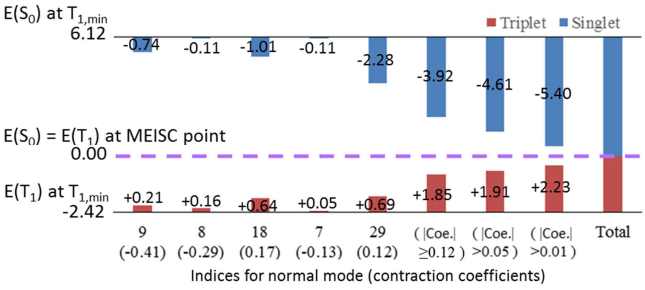

Figure 9 Energy changes of the S_0 and T_1 states introduced by structural change from the T_1 minimum to the MEISCP. Unit is in kcal/mol. The structural change was expressed by a linear combination of normal mode vector at the T_1 minimum. The upper and lower lines denote the energy levels of the triplet and singlet states at the T_1 minimum, respectively. Energy changes of T_1 and S_0 states caused by the structural change were represented with red and blue bars, respectively. Calculations were carried out with the B3LYP functional.

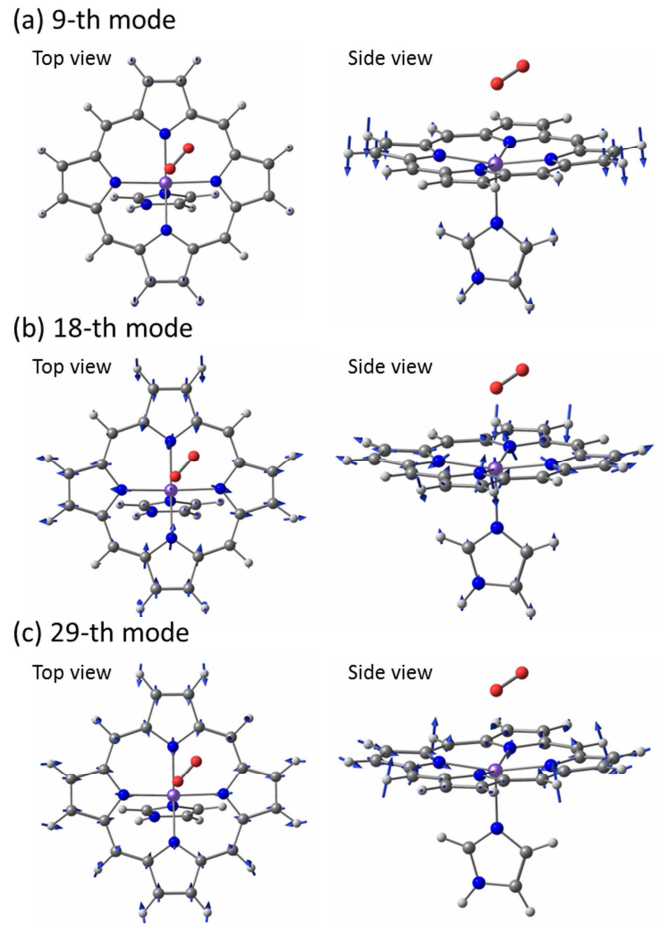

Figure 10 Ninth, eighteenth, and twenty-ninth normal mode at the T_1 minimum.

One striking feature is the contribution of the 29-th component. Even though the expansion coefficient is only 0.12, this mode effectively changes the energy difference between the S_0 and T_1 states. The energy of the S_0 state becomes lower by about 2 kcal/mol, and that of the T_1 state becomes higher by about 1 kcal/mol. In particular, the amount of the stabilization in the S_0 state is large. As shown in Figure 10, the structural change by the 29-th component is symmetric shrinking of tetrapyrrole unit. We note that no explicit change in the Fe-O_2 distance was involved. In this sense, this symmetric shrinking of the tetrapyrroles is one of the most important reaction coordinates for controlling the relative energy difference between the singlet and triplet states.

Conclusions

Intersystem crossing pathway of the O_2 binding to FePorIm was investigated with the RASPT2 and DFT calculations. The RASPT2 single-point calculations at the DFT(B97D) optimized structures were performed. At longer Fe-O distances, the relative energy of S_0 state from T_1 states was well separated. The present result indicates that the probability of the ISC at these structures, namely the broad-crossing mechanism, would be possible, but not significant.

The S_0/T_1 MEISCP was determined using a constraint optimization method. The Fe-O distance of the MEISCP was 2.17 Å, and Fe atoms are almost on the porphyrin plane. To the MEISCP from the T_1 minimum, calculated energy barrier is 1.0 kcal/mol by DFT(B97D) and more than 2 kcal/mol by RASPT2. Therefore, the crossing point constitutes transition state of the O_2 binding, and the spin-change barrier mechanism is better ascribed than the broad crossing mechanism. The B3LYP functional also gives the similar result, but the Fe-O distance of the MEISCP is longer by about 0.6 Å. Single-point MS-CASPT2 calculations were also performed along the steepest descent reaction pathway calculated by DFT(B97D). In the MS-CASPT2 result, the S_0 and T_1 states cross at the Fe-O distance of 2.05 Å, which reasonably agrees with the DFT(B97D) result.

To analyse the reaction coordinate from T_1 minimum to the MEISCP, we expand the structure change in terms of the normal mode at T_1 minimum structure. In addition to the Fe-O stretching mode, symmetric shrinking of porphyrin ring contributes to the structure change. Energy decomposition analysis was also carried out to figure out energy change caused by each structure change. It turned out that the shrinking of the porphyrin ring explains more than 1/3 of energy change from T_1 minimum to MEISCP. The result indicates that even though the reaction is O_2 binding, reaction coordinates that control the relative energy plays a key role in spin-state changing reactions.

Acknowledgements

This study was supported by JST-CREST and JSPS KAKENHI Grant Number 15H05805. AN is supported by JSPS KAKENHI Grant Number 15K06563, and NN is supported by JSPS KAKENHI Grant Number 15K20832 and 15H03770. A part of the study was also supported by the FLAGSHIP2020, MEXT within the priority study5 (Development of new fundamental technologies for high-efficiency energy creation, conversion/storage and use). A part of the computations was carried out at RCCS (Okazaki, Japan) and ACCMS (Kyoto University).

Notes and references

1. M. Momenteau and C. A. Reed, *Chem. Rev.*, 1994, **94**, 659-698.
2. H. Chen, W. Lai and S. Shaik, *J. Phys. Chem. B*, 2011, **115**, 1727-1742.
3. L. Pauling and C. D. Coryell, *Proc. Natl. Acad. Sci. U.S.A.*, 1936, **22**, 210-211.
4. J. W. Petrich, C. Poyart and J. L. Martin, *Biochemistry-Us*, 1988, **27**, 4049-4060.
5. K. N. Walda, X. Y. Liu, V. S. Sharma and D. Magde, *Biochemistry-Us*, 1994, **33**, 2198-2209.
6. M. D. Chatfield, K. N. Walda and D. Magde, *J. Am. Chem. Soc.*, 1990, **112**, 4680-4687.
7. J. J. Weiss, *Nature*, 1964, **202**, 83-84.
8. W. A. Goddard, III and B. D. Olafson, *Proc. Natl. Acad. Sci. U.S.A.*, 1975, **72**, 2335-2339.
9. B. D. Olafson and W. A. Goddard, III, *Proc. Natl. Acad. Sci. U.S.A.*, 1977, **74**, 1315-1319.
10. S. Yamamoto and H. Kashiwagi, *Chem. Phys. Lett.*, 1989, **161**, 85-89.
11. R. D. Harcourt, *Chem. Phys. Lett.*, **167**, 374-377.
12. K. P. Jensen, B. O. Roos and U. Ryde, *J. Inorg. Biochem.*, 2005, **99**, 45-54.
13. K. P. Jensen, B. O. Roos and U. Ryde, *J. Inorg. Biochem.*, 2005, **99**, 978-978.
14. J. Ribas-Arino and J. J. Novoa, *Chem. Comm.*, 2007, 3160-3162.
15. H. Chen, M. Ikeda-Saito and S. Shaik, *J. Am. Chem. Soc.*, 2008, **130**, 14778-14790.
16. H. Nakatsuji, J. Hasegawa, H. Ueda and M. Hada, *Chem. Phys. Lett.*, 1996, **250**, 379-386.
17. K. P. Jensen and U. Ryde, *J. Biol. Chem.*, 2004, **279**, 14561-14569.
18. K. P. Kepp, *ChemPhysChem*, 2013, **14**, 3551-3558.
19. S. Franzen, *Proc. Natl. Acad. Sci. USA*, 2002, **99**, 16754-16759.
20. H. Nakashima, J. Hasegawa and H. Nakatsuji, *J. Comput. Chem.*, 2006, **27**, 426-433.
21. M. E. Ali, B. Sanyal and P. M. Oppeneer, *J. Phys. Chem. B*, 2012, **116**, 5849-5859.
22. M. Reiher, O. Salomon and B. A. Hess, *Theor Chem Acc*, 2001, **107**, 48-55.
23. P. E. M. Siegbahn, M. R. A. Blomberg and S.-L. Chen, *J. Chem. Theo. Comp.*, 2010, **6**, 2040-2044.
24. R. Poli and J. N. Harvey, *Chem. Soc. Rev.*, 2002, **32**, 1–8.
25. S. Shaik, D. Danovich, A. Fiedler, D. Schröder and H. Schwarz, *Helv. Chim. Acta*, 1995, **78**, 1393-1407.
26. D. Schröder, S. Shaik and H. Schwarz, *Acc. Chem. Res.*, 2000, **33**, 139-145.
27. C. R. Johnson, D. W. Ownby, S. J. Gill and K. S. Peters, *Biochemistry-Us*, 1992, **31**, 10074–10082.
28. N. Koga and K. Morokuma, *Chem. Phys. Letters*, 1985, **119**, 371-374.
29. J. N. Harvey, M. Aschi, H. Schwarz and W. Koch, *Theor. Chem. Acc.*, 1998, **99**, 95-99.
30. A. D. Becke, *J. Chem. Phys.*, 1997, **107**, 8554-8560.
31. S. Grimme, *J. Comp. Chem.*, 2006, **27**, 1787-1799.
32. M. Dolg, U. Wedig, H. Stoll and H. Preuss, *J. Chem. Phys.*, 1987, **86**, 866-872.
33. R. Krishnan, J. S. Binkley, R. Seeger and J. A. Pople, *J. Chem. Phys.*, 1980, **72**, 650.
34. P. C. Hariharan and J. A. Pople, *Theoret. Chem. Acta*, 1973, **28**, 213.
35. B. O. Roos, R. Lindh, P.-Å. Malmqvist, V. Veryazov and P.-O. Widmark, *J. Phys. Chem. A*, 2005, **108**, 2851.
36. B. O. Roos, R. Lindh, P.-Å. Malmqvist, V. Veryazov and P.-O. Widmark, *J. Phys. Chem. A*, 2005, **109**, 6575-6579.
37. N. Forsberg and P.-Å. Malmqvist., *Chem. Phys. Letters*, 1997, **274**, 196-204.

38. A. Nakayama, Y. Harabuchi, S. Yamazaki and T. Taketsugu, *Phys. Chem. Chem. Phys.*, 2013, **15**, 12322-12339.
39. B. G. Levine, J. D. Coe and T. J. Martínez, *J. Phys. Chem. B*, 2008, **112**, 405-413.
40. M. J. Frisch, G. W. Trucks, H. B. Schlegel, G. E. Scuseria, M. A. Robb, J. R. Cheeseman, G. Scalmani, V. Barone, B. Mennucci, G. A. Petersson, H. Nakatsuji, M. Caricato, X. Li, H. P. Hratchian, A. F. Izmaylov, J. Bloino, G. Zheng, J. L. Sonnenberg, M. Hada, M. Ehara, K. Toyota, R. Fukuda, J. Hasegawa, M. Ishida, T. Nakajima, Y. Honda, O. Kitao, H. Nakai, T. Vreven, J. J. A. Montgomery, J. E. Peralta, F. Ogliaro, M. Bearpark, J. J. Heyd, E. Brothers, K. N. Kudin, V. N. Staroverov, R. Kobayashi, J. Normand, K. Raghavachari, A. Rendell, J. C. Burant, S. S. Iyengar, J. Tomasi, M. Cossi, N. Rega, J. M. Millam, M. Klene, J. E. Knox, J. B. Cross, V. Bakken, C. Adamo, J. Jaramillo, R. Gomperts, R. E. Stratmann, O. Yazyev, A. J. Austin, R. Cammi, C. Pomelli, J. W. Ochterski, R. L. Martin, K. Morokuma, V. G. Zakrzewski, G. A. Voth, P. Salvador, J. J. Dannenberg, S. Dapprich, A. D. Daniels, Ö. Farkas, J. B. Foresman, J. V. Ortiz, J. Cioslowski and D. J. Fox, *Journal*, 2009.
41. H.-J. Werner, P. J. Knowles, G. Knizia, F. R. Manby and M. Schütz, *WIREs Comput. Mol. Sci.*, 2012, **2**, 242-253.
42. H.-J. Werner, P. J. Knowles, G. Knizia, F. R. Manby, M. Schütz, P. Celani, T. Korona, R. Lindh, A. Mitrushenkov, G. Rauhut, K. R. Shamasundar, T. B. Adler, R. D. Amos, A. Bernhardsson, A. Berning, D. L. Cooper, M. J. O. Deegan, A. J. Dobbyn, F. Eckert, E. Goll, C. Hampel, A. Hesselmann, G. Hetzer, T. Hrenar, G. Jansen, C. Köppl, Y. Liu, A. W. Lloyd, R. A. Mata, A. J. May, S. J. McNicholas, W. Meyer, M. E. Mura, A. Nicklass, D. P. O'Neill, P. Palmieri, D. Peng, K. Pflüger, R. Pitzer, M. Reiher, T. Shiozaki, H. Stoll, A. J. Stone, R. Tarroni, T. Thorsteinsson and M. Wang, *Journal*, 2012.
43. F. Aquilante, L. D. Vico, N. Ferré, G. Ghigo, P.-Å. Malmqvist, P. Neogrády, T. B. Pedersen, M. Pitonak, M. Reiher, B. O. Roos, L. Serrano-Andrés, M. Urban, V. Veryazov and R. Lindh, *J. Comp. Chem.*, 2010, **31**, 224-247.
44. S. Shaik and H. Chen, *J. Biol. Inorg. Chem.*, 2011, **16**, 841-855.
45. M. Radon and K. Pierloot, *J. Phys. Chem. A*, 2008, **112**, 11824-11832.
46. S. Vancoillie, H. Zhao, M. Radon and K. Pierloot, *J. Chem. Theo. Comp.*, 2010, **6**, 576-582.
47. F. A. Hamprecht, A. Cohen, D. J. Tozer and N. C. Handy, *J. Chem. Phys.*, 1998, **109**, 6264-6271.
48. P.-Å. Malmqvist, *Int. J. Quantum Chem.*, 1986, **30**, 479-494.
49. P.-Å. Malmqvist and B. O. Roos, *Chem. Phys. Letters*, 1989, **155**, 189-194.